Longshore drift produced by climate-modulated monsoons and typhoons in the South China Sea

Patrick Marchesiello, Elodie Kestenare, Rafael Almar, Julien Boucharel, Nguyet Minh Nguyen

Version of Record: https://www.sciencedirect.com/science/article/pii/S0924796320300956
Manuscript_aa2afbdbf5ec48150b377be25c21b05c

Longshore drift produced by climate-modulated monsoons and typhoons in the South China Sea

Patrick Marchesiello[a,c,*], Elodie Kestenare[a], Rafael Almar[a], Julien Boucharel[b], Nguyet Minh Nguyen[d]

[a] *IRD/LEGOS, 14 av. Edouard Belin, 31400 Toulouse, France*
[b] *CNRS/LEGOS, 14 av. Edouard Belin, 31400 Toulouse, France*
[c] *CARE center, Ho Chi Minh City Univ. of Technology, HCMC, Vietnam*
[d] *Southern Institute of Water Resources Research, HCMC, Vietnam*

Abstract

Monsoons and typhoons impact the tropical coastal zones through their signature on winds and waves, leading to increased vulnerability – through erosion, marine submersion and flooding – of an ever growing coastal population. This study addresses wave-driven coastal impacts in the South China Sea (SCS), particularly along the Vietnam coast. Using 38 years of offshore wave fields from ERA-Interim reanalysis, we assess the seasonal and interannual variability of wave patterns, storminess, and wave-induced alongshore sediment transport (longshore drift). Results suggest a large seasonal coastal impact due to high-energy, north-easterly waves generated by winter monsoon winds. The net annual sediment transport is southward with significant interannual and decadal variations (20% standard deviation with particular years at 40% of the mean), presenting strong correlations with the El Niño Southern Oscillation (ENSO) and Pacific Decadal Oscillation (PDO) regime changes. The regime shift of 1998, from a warm to a cold PDO phase characterized by more La Niña events, is associated with an increase in winter wave energy and thus higher sediment transport (about 10%). The typhoon activity in the SCS is partly associated with that of the Pacific Northwest basin, but as a large semi-enclosed sea, presents local differences. It is positively correlated with La Niña in summer and with El Niño Modoki in winter. The summer correlation to ENSO phases is opposite to that of the whole Northwest Pacific due to competing local and remote mechanisms driving cyclone formation and trajectory. For the same reason, the effects of ENSO and PDO phases are opposite in the SCS: during

the last cold PDO phase, typhoon frequency was reduced by 20%, with significant net impact on estimated sediment transport. The typhoon contribution to sediment transport is a 15% reinforcement of southward transport due essentially to winter activity. If winter monsoon and typhoons appear to work together on average, their low-frequency variability are out-of-phase. This is particularly clear at decadal scale, as cold PDO phases seem favorable to strong winter monsoon waves but detrimental to SCS typhoon numbers. These results confirm that regional climate variability (together with human factors affecting river sediment supply, coastal management of beach-dune systems, land subsidence, mangrove deforestation) is an essential part of coastal vulnerability that needs to be better assessed.
Keywords: longshore drift, wave climate, monsoon, typhoon, ENSO, PDO

1. Introduction

The South China Sea (SCS; or Vietnam East Sea in Vietnam), is the largest semi-enclosed marginal sea in the Northwest Pacific and a source of interest for surrounding countries, including Vietnam, a coastal state within a tropical monsoon area (Fig. 1). Its coastal zone shelters many cities with a growing population that is now threatened by erosion and submersion. Various engineering projects have investigated coastal vulnerability but general assessments on the status of erosion along the Vietnam coast are relying on scarce data (e.g., FAO report by Ngo et al. 2006, and more recently Hue and Thanh 2020) or derived from satellite estimations over the last three decades (Luijendijk et al., 2018). The coast is generally split into three main regions: northern, central (between 11°N and 19°N) and southern. Coastal erosion and accretion are believed to vary from one region to the other according to river sediment supply, lithologic composition of the coast, human factors[1], and oceanic conditions.

*Corresponding author
Email address: patrick.marchesiello@ird.fr (Patrick Marchesiello)

[1]The list of human factors is long, spanning from the watershed to the coastal zone: dam construction, embankment, irrigation, mining, forest-to-agriculture conversion, groundwater extraction, coastal development (ports, resorts, channel dredging, groins and breakwaters), mangrove deforestation, etc

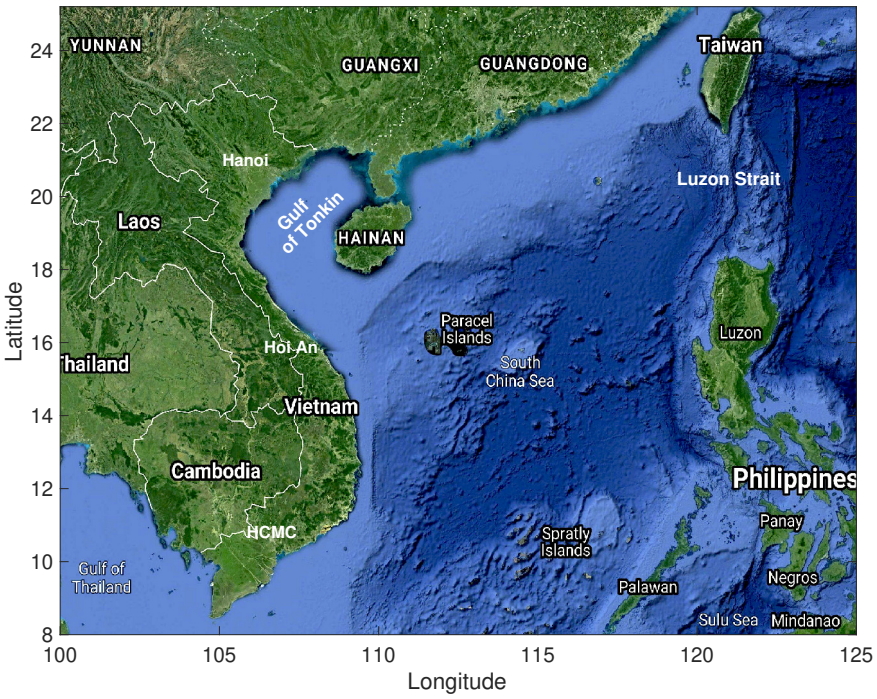

Figure 1: Geographical map of the South China Sea region.

The northern region located in the Gulf of Tonkin and protected from most SCS swell conditions (Nguyen et al., 2014) is usually associated with sedimentation and will thus be discarded in this study. In the central region, erosion has been observed in all coastal provinces due to a more direct exposition to swell and local wind waves. Sand being the main shore-building material, the strongest erosion is expected to occur in convex coastal sections of the coast facing wind and wave direction (Komar, 1976). The main focus of the paper will be on the sandy central coast, which has the longest stretch and largest angle with dominant incoming swell. We will ignore the Mekong delta coastal zone in the southern region, which is also highly vulnerable to oceanic conditions but presents specific conditions as a lowland, mud-dominated system (the delta is about 1 m above sea level; Minderhoud et al. 2019). In particular, sediment transport mechanisms in the coastal delta are very different from a sand-dominated shoreline as they are affected by wide and shallow mudflats (Marchesiello et al., 2019).

Coastal morphological evolution is generally examined at seasonal and synoptic (storm-

driven) timescales, while a few studies (Bryan et al., 2008; Mortlock and Goodwin, 2016) show that morphological adjustment can occur at lower frequencies (and may be larger than short-term variations). The long-term ocean wave climate has only been recently investigated in the SCS due to limited data before the 1980s (Chu et al., 2004; Mirzaei et al., 2013). With the development of satellite observation, numerical modeling and data assimilation techniques, reanalyzes have progressively been available for marine climate research. These products show that the SCS coastal region is mostly affected by long-period swells that travel from the Northeast in winter, although local wind waves have a significant role as well. Besides a seasonal effect, tropical beaches are also exposed to infrequent short (1–3 days) but paroxysmal typhoons. Almar et al. (2017) show that if a storm can produce strong offshore sediment transport in Nha Trang (about 16°N), central Vietnam, the beach would slowly recover under persisting low to moderate waves during the rest of the year. However, any residual alongshore transport would lead to morphological adjustment. Low-frequency variability of winds and waves can also impact the coastal zone through modulation of surging seas and typhoon rainfall and floods. Here, we will focus on longshore sediment transport and tentatively use it as a climatic index of erosion potential.

In this paper, we follow the methodology presented in Almar et al. (2015) for the Gulf of Guinea in West Africa to connect the large-scale climate variability to the drivers of coastal vulnerability in Vietnam, as diagnosed by longshore sediment transport. The reliable global reanalyses from ERA-Interim (ERA-I), covering almost four decades, will bring new insights on the statistical connection between coastal vulnerability and climate variability, from typhoon and monsoons intraseasonal events, to seasonal monsoon conditions, interannual El Niño Southern Oscillation (ENSO), and Pacific Decadal Oscillation (PDO). This analysis will also reveal environmental factors that may predominantly affect shoreline variability in relation with ENSO and PDO. Ultimately, it will help us to foresee changes of coastal impacts in the coming decade.

2. Data and methodology

2.1. Wave reanalysis

We used ERA-I bulk wave parameters (significant height Hs, peak period Tp and direction of both swell and wind waves) extracted from the ECMWF data server on a 0.5° grid, with a 6-h temporal resolution over the period 1979-2016 (Dee et al., 2011). In ERA-I, the analysis of surface parameters is performed separately from the main atmospheric analysis. An optimal interpolation (OI) analysis of ocean wave height is performed using data from space-borne radar altimeters, when available (starting in 1991). This analysis is then used to correct the first-guess spectrum, which is generated by the wave forecast model (Lionello et al., 1992; Dee et al., 2011). The latter consists of a fully coupled wave model (the ECMWF Wave Atmospheric Model WAM) describing the evolution of two-dimensional wave spectra. ERA-40 and following ERA-I are the first reanalyzes featuring an ocean wind-wave model coupled to the atmosphere, and the quality of the wave data has been validated against buoy and altimeter data (Sterl and Caires, 2005; Stopa and Cheung, 2014). There is generally good correlation between the reanalysis and observational data, apart from the extreme cases of very high waves ($H_s > 5$ m) or very small waves ($H_s < 1$ m), which tend to be under- or overestimated respectively. These extreme wave conditions are infrequent in the Vietnam East Sea but not absent, due to tropical storms. The Vietnam coast experiences 8-10 tropical storms each year in average (Wang et al., 2007), which may account for part of beach erosion as we will discover. Let's keep in mind that the largest storm swell is probably underestimated in ERA-I data.

2.2. Typhoon database and clustering

The trajectories and intensities of typhoons are extracted from the best track archives provided by NOAA's Tropical Prediction Center. Here we call tropical cyclones (TCs) all tropical storms with 10-minute maximum sustained winds greater than 17 m/s (34 kn or 63 km/h), while typhoons are mature cyclonic systems with winds greater than 33 m/s (64 kn or 119 km/h). To evaluate cyclonic activity, we use a density index, which is calculated as the monthly number of TCs in a [5° × 5°] sliding box covering the entire North-West

Pacific basin at a $[1^\circ \times 1^\circ]$ resolution. This calculation is detailed in Almar et al. (2019) and Boucharel et al. (2016) for the Atlantic and Eastern Pacific basins respectively.

Following Bell et al. (2019), we applied the probabilistic curve-clustering technique of Gaffney et al. (2007) to group together TC tracks of similar properties (initial conditions and track curvature). An advantage of clustering TC tracks is that different but overlapping track types (with different curvature) can be analyzed separately. Twenty-five cluster runs were performed for the SCS where the input order of the tracks was randomized and 12 expected maximization starts were used. The cluster run with the smallest trained log-likelihood value was selected. Linear regression mixture models were fitted to TC tracks with an objectively determined number of clusters. Bell et al. (2019) find an optimized total of 9 clusters in the entire Northwestern Pacific (NWP) TC region, including 2 in the China sea; hence our choice of 2 clusters in this region (Fig. 6b).

2.3. Environmental variables

Vertical wind shear (VWS), sea surface temperature (SST), and mid-troposphere relative humidity are among the most commonly used environmental variables by the scientific community to assess the environmental control of TC genesis and intensity (Camargo et al., 2010). The VWS, defined as the environmental horizontal wind difference between 200- and 850-hPa pressure levels (DeMaria, 1996) and relative humidity, averaged between 700- and 850-hPa pressure levels (Kaplan and DeMaria, 2003; Wu et al., 2012), are extracted from the NCEP/NCAR reanalysis data. The SST is taken from the ECMWF Ocean Reanalysis System 3 (ORA-S4) (Balmaseda et al., 2013). All variables are monthly averaged and interannual monthly anomalies are computed with respect to a monthly mean climatology (interannual variability is obtained by averaging monthly anomalies over each year).

2.4. Sediment transport formulation

Here, as in Almar et al. (2015), we use the relatively recent Kaczmarek et al. (2005) formula (Eq.1 below) for its suitability in various conditions. The longshore sediment volume

transport is computed as:

$$\begin{aligned} Q &= 0.023 - H_b^2\ V \qquad \text{if } H_b^2\ V < 0.15 \\ Q &= 0.00225 + 0.008 H_b^2\ V \quad \text{if } H_b^2\ V > 0.15 \end{aligned} \tag{1}$$

H_b is the breaking wave height (see below) and V an estimated surf zone long shore current derived from the commonly used Longuet-Higgins formula:

$$V = 0.25 K_v\ \sqrt{\gamma g H_b}\ sin2\alpha_b \tag{2}$$

α_b is wave angle, $\gamma = H_b/D_b = 0.78$ the constant breaker index following Battjes and Janssen (1978), g=9.8 m/s^2 the gravitational acceleration, D_b the local water depth, and K_v an empirical constant. We use $K_v = 2.9$, as in Almar et al. (2015), for wave-dominated, sandy environments. We calculated monthly and annual values of the longshore sediment transport associated with the total wave field (wind and swell waves).

Note that this estimation of longshore drift can only provide an order of magnitude rather than an exact quantitative assessment (Pilkey and Cooper, 2002), but the study focuses on transport sensitivity to oceanic forcing variability. Assuming that coastal erosion (or accretion) results primarily from the longshore gradient of sediment transport, it should broadly vary as the sediment transport itself. In this sense, our transport formulation can be used as a climatic index of erosion potential.

3. Results: monsoon and typhoon impacts with ENSO/PDO modulation

3.1. Monsoons

Waves are generally most energetic in higher latitudes, although the tropical band can also experience large waves, like those associated with monsoon weather that impact the coasts of southeastern Asia (Felix et al., 2019). The seasonal climatology of the combined wind sea and swell waves obtained by seasonally averaging all waves over the period 1979–2016 is presented in Figure 2. The wave field reflects the Asian monsoon weather (for a review, see Chang et al. 2006). Summer monsoon appears to drive low-energy, short-period

southwesterly waves. However, the onset of northeast winter monsoon (October-April) resulting from the formation of the Siberian High leads to high wind conditions, particularly off northern and central Vietnam. It can bring strong persistent swell of somewhat lower energy but longer duration than tropical storms. Swell and wind waves follow a similar seasonal pattern, with swell generally larger than wind waves. In winter, the mean wind magnitude over the SCS is about 9 m/s (not shown) and the resulting swell has monthly mean significant wave heights of 1-2.5 m for swell propagating from the northeast (50° angle to the north) with a mean period of more than 8 s. The winter monsoon swell is associated with a long fetch that extends along the SCS and beyond through the Luzon Strait (between Taiwan and Luzon island of the Philippines that connects the SCS to the Pacific basin; Fig. 1). Wind waves present larger intraseasonal variations, especially during winter, for both magnitude and direction (not shown).

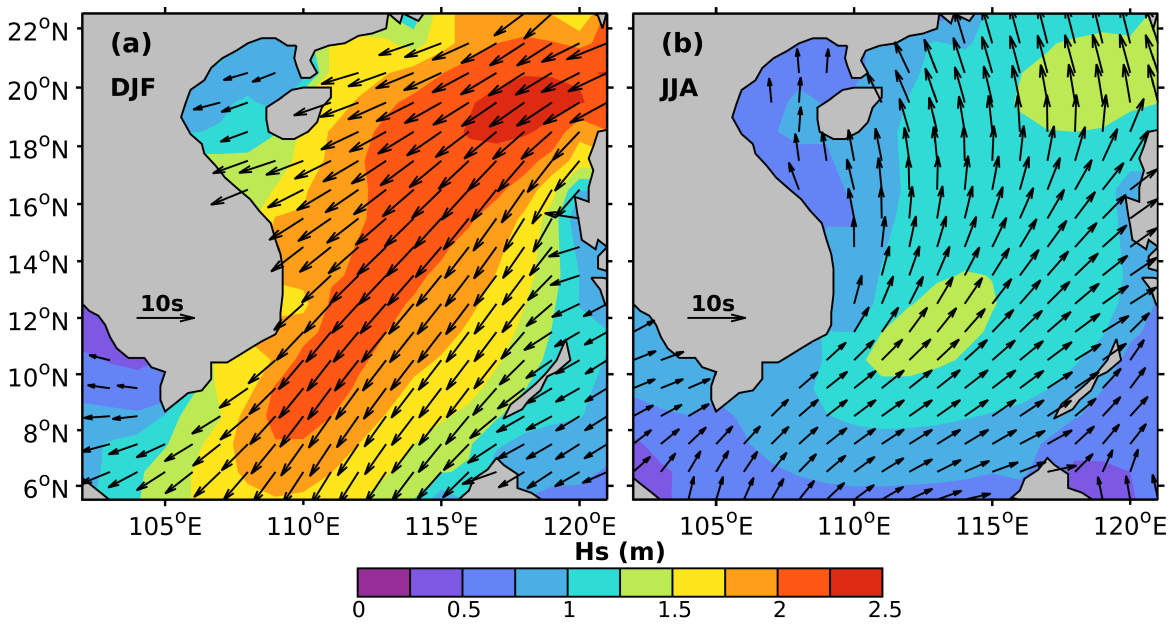

Figure 2: Winter (December-February; left) and summer (June-August; right) wave characteristics: Hs (color); wave direction (vector direction) and period (vector magnitude)

As the Siberian High varies on timescales of a few days to a week, surges of northeast

winds set in then wane with this cycle (Shoji et al., 2014). ERA-I presents heavy swells (> 4 m) during winter monsoon surges (not shown). There is substantial literature on the atmospheric cold intrusion — called cold surges — affecting the Southeast Asian coastal states every winter (Shoji et al., 2014; Chang et al., 2006), but comparatively little about the effect of these energetic events on the sea state (Almar et al., 2017). In contrast during summer, weaker southwesterly winds of about 6 m/s dominate over most parts of the SCS, consistent with previous studies (Chu et al., 2004; Mirzaei et al., 2013). Although, as already mentioned, summer monsoon drives weak southwesterly waves (0.8 m in average), tropical storms and typhoons can cause significant wave heights to rise briefly to around 4 m.

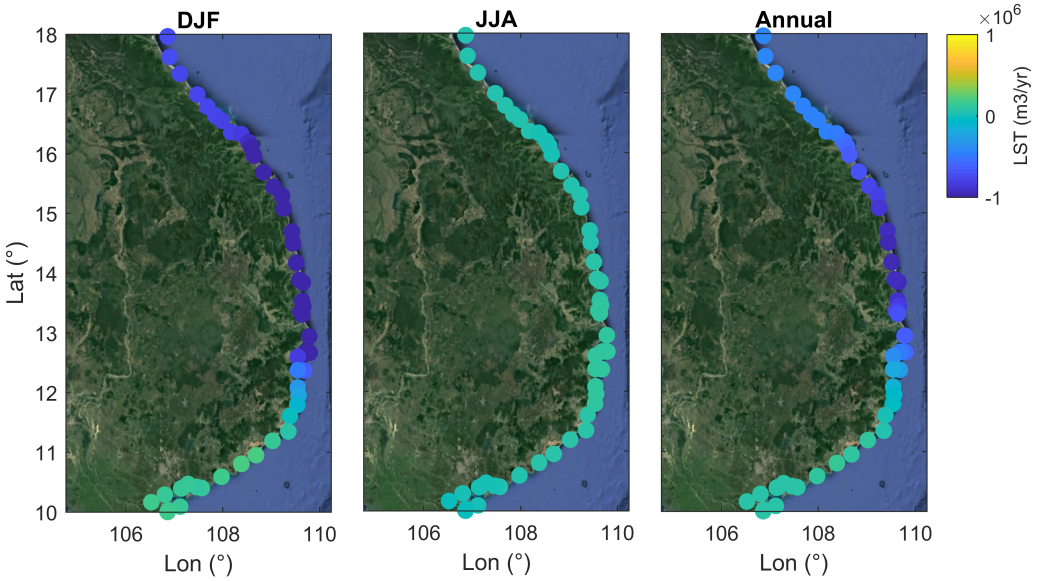

Figure 3: Winter (DJF), Summer (JJA), and Annual mean longshore sediment transport along the Vietnam coast calculated from ERA-I wave fields and Kaczmarek formulation. Southward transport is negative.

3.1.1. Mean, seasonal and interannual sediment transport

We now evaluate the wave-induced longshore sediment transport along the Vietnamese coast. According to the Kaczmarek formulation, the oblique strong winter swell largely dominates an annual mean southward sediment transport of about 0.5-1 million m^3/year over the central coast (Fig. 3). This is a relatively high value generally associated with drift-aligned beach morphology (Bird, 2005) and consistent with long sandy shores characteristic

of Vietnam's central coast (Hue and Thanh, 2020).

There are large seasonal and interannual variations in sediment transport. Interannual variations have a standard deviation of about 20 % of the mean (Fig. 4) and present significant correlations (about 55%) with Nino3.4 index anomalies[2], one of the most commonly used indices to characterize the El Niño Southern Oscillation (Trenberth and Stepaniak, 2001). El Niño events are characterized by surface warming of the central and eastern tropical Pacific Ocean and weakening of equatorial trade winds that occur every few years. Alternating warm El Niño and cold La Niña phases, referred to as ENSO, represent the largest year-to-year fluctuation of the global climate system (McPhaden et al., 1998). Figure 5 presents El Niño and La Niña wind patterns constructed from composites of all positive and negative ENSO events during 1979-2016. In the SCS, the negative ENSO phase (La Niña) produces a cyclonic anomaly in the wind regime. Therefore, La Niña events are associated with increased winter monsoon wave energy (not shown) and resulting southward longshore transport anomalies (of about 40% for the 1999 and 2011 episodes compared to the annual mean). Conversely, El Niño events produce weaker waves and transport, particularly during the strong El Niño events of 1997 and 2015.

3.1.2. Decadal modulation

At longer time scales, Figure 4 also reveals a PDO signature, i.e. the dominant mode of climate variability at decadal time scales in the North Pacific (Mantua et al., 1997; Mantua and Hare, 2002). Sediment transport time series exhibit a shift around the strong 1997-98 El Niño event. During the first part of the record (1979 to 1998), PDO is in its warm phase, characterized by a cooler Northwest Pacific ocean and stronger El Niño events with more frequent occurrence of the Eastern Pacific (EP) type. Typically, EP Niños exhibit an intense warming pattern confined to the Eastern Pacific, while Central Pacific (CP) Niños

[2]The Nino3.4 index is based on tropical Pacific SST anomalies averaged over the central equatorial Pacific [5N-5S, 170W-120W], where key ocean-atmosphere interactions for ENSO occur. Anomalies are computed using a 5-month running mean, and El Niño or La Niña events are defined when these anomalies exceeds ± 0.4C for a period of six months or more.

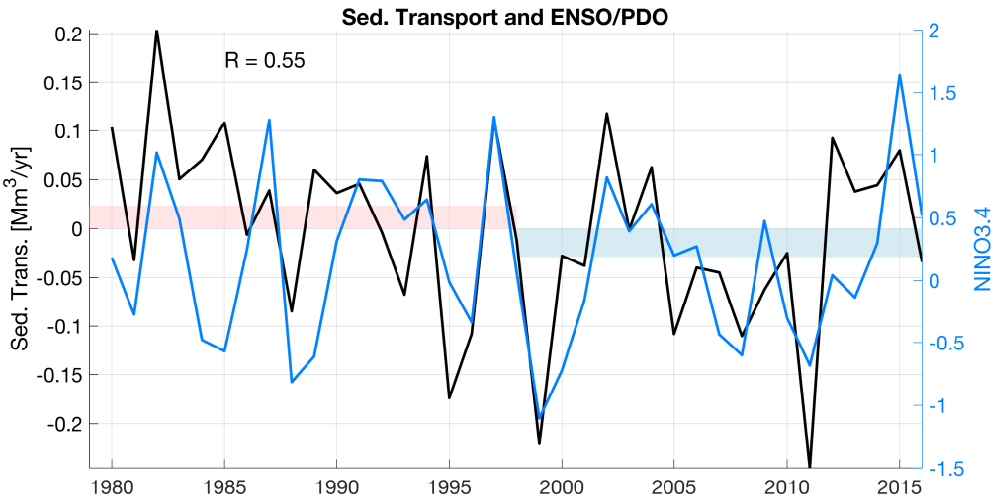

Figure 4: Yearly anomalies of longshore sediment transport along the central coast (around Hoi-An) calculated from ERA-I wave fields and Kaczmarek formulation (the mean southward transport shown in Fig. 3 is removed and the standard deviation of interannual variations is about 20% of this mean). Transport anomalies are compared with interannual (ENSO: Nino3.4 index anomaly) and decadal (PDO) variability. The correlation with Nino3.4 is about 55% (with 95% confidence). For the relation with PDO, the mean sediment transports over the warm (1979-1998) and cold (1999-2016) PDO phases are shown with light red and blue colors, indicating northward (southward) anomalies. The transport increased in average by about 10% of the mean between PDO phases (3 times larger than the standard error on the mean).

(or El Niño Modoki) are characterized by moderate warming around the dateline (Capotondi et al., 2015). These different flavors of events, which express ENSO diversity, have distinct features, impacts and remote connections. The second half of the record (1999 to 2016) is marked by a negative PDO phase, which favors frequent and strong La Niña events due to a warmer ocean background in the Northwest Pacific. During this recent cold phase, there were twice as many years with southward sediment transport anomalies in central Vietnam and the transport increased in average by 0.05 Mm^3/yr between the two phases (3 times larger than the standard error on the mean), i.e., about 10% of the mean transport. Therefore, in the SCS, the two most recent decades are characterized by a cold PDO phase that promoted higher wave energy due to an enhanced La Niña effect on winter monsoon activity, increasing the general southward sediment transport along Vietnam. We conclude that decadal/multi-decadal variations (associated with PDO and more generally any ENSO

low-frequency modulation) can be a major driver of erosion processes along the Vietnamese coast.

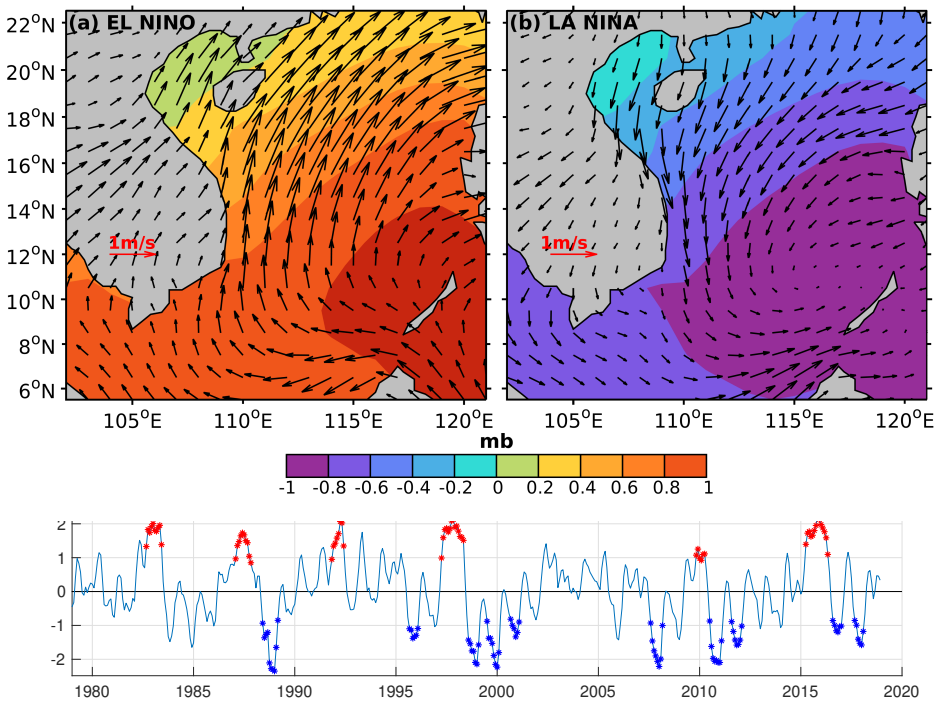

Figure 5: Wind anomalies related to El Niño (left) and La Niña (right), constructed from composites of events: wind magnitude and direction anomaly (vector); surface air pressure anomaly (color). The bottom panel presents the Nino3.4 index anomaly (detrended) with El Niño (red dots) and La Niña (blue dots) events used in the composites. The warm and cold PDO phases before or after 1998 are marked by a prevalence of El Niño and La Niña events respectively.

3.2. Typhoons

The Northwestern Pacific ocean is the most active tropical cyclone basin in the world with an annual average of about 25 TCs, i.e., a third of global activity (Lin et al., 2020). As a reminder (methodology section), we call TCs all tropical storms with 10-minute sustained wind speed greater than 17 m/s (34 kn or 63 km/h), while typhoons are stronger cyclonic systems with winds greater than 33 m/s (64 kn or 119 km/h). Over the SCS, the annual mean TC number in our data is about 10, comprising 6 typhoons. Of these storms, about a third is generated locally, as in Wang et al. (2007). TCs generated over the NWP are

strongly influenced by the large-scale atmospheric circulation and oceanic environment (Lin et al., 2020), but TCs generated over the SCS are subject to a more local set of dynamical and thermodynamical factors, which may be at odds with the large-scale influence (Elsner and Liu, 2003; Ling et al., 2015). Our results confirm and further refine these findings.

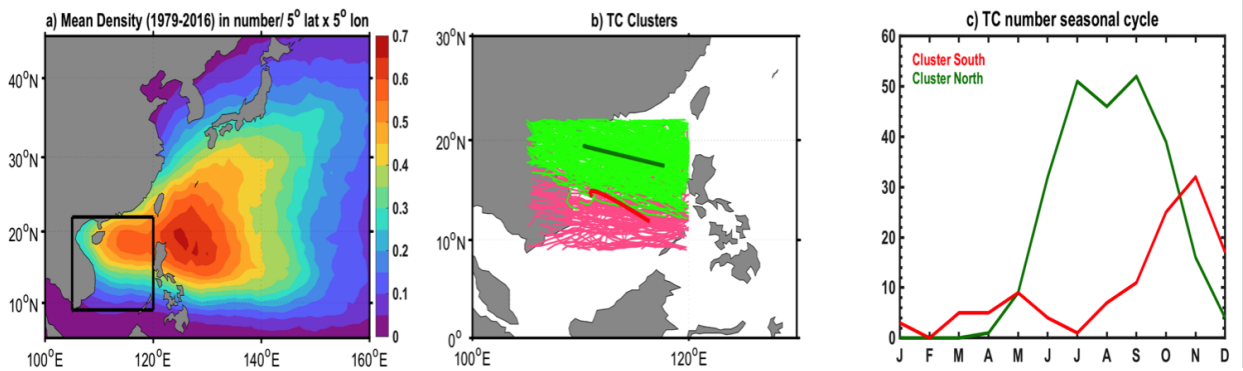

Figure 6: TC density and clustering in the SCS; a) mean annual storm density over the period 1979-2016 in the northwestern Pacific basin; b) TC tracks of the two main clusters in the SCS: green tracks for Cluster North in northern SCS; and red tracks for Cluster South in southern SCS (mean tracks of each cluster are superimposed in bold lines); c) monthly TC frequency for each cluster.

Figure 6a shows the mean annual TC density over the period 1979-2016 in the NWP basin. TC activity is largest in the northern part of the SCS, locally generated or resulting from TCs in the NWP that are taking a straight westward route though the Philippines archipelago. To refine these statistics, we applied the probabilistic curve-clustering technique presented in the methodology section. Two clusters are selected in the SCS (Fig. 6b). It appears that the dominant cluster (green) mainly accounts for northern TC tracks, which prevail in summer (Fig. 6c), while the second cluster (red) is representative of southern tracks that occur more often in the early winter season (Nov-Dec) as wind shear and cold SST become detrimental to TC intensification in the northern SCS (Wang et al. 2007; these conditions spread south as winter progresses). These clusters will be referred to as "Cluster North" and "Cluster South" respectively in the remainder of the paper. Typhoon Linda is an infamous member of Cluster South as it made landfall in the Mekong delta in November 1997 and was declared the worst storm in recent Vietnam history due to human loss in this

vulnerable low-level elevation zone (Anh et al., 2017).

3.2.1. Interannual modulation

Figure 7 presents a time series of SCS TC number from 1979 to 2016, showing large interannual and decadal variability. The correlation between TC count and Nino3.4 is -0.33 (with 95% confidence) and is therefore out of phase with variability in the whole Pacific basin (Zhao and Wang, 2019). To explain this result, previous studies hypothesized various ENSO-TC relationship mechanisms (e.g., Ling et al. 2015; Wang et al. 2007), one of them – called ENSO-typhoon hypothesis – standing out by successfully relating SCS TC activity to changes in NWP TC tracks (Elsner and Liu, 2003). The hypothesis states that TC formation during an El Niño event shifts eastward, with more typhoons tending to head north and staying away from the SCS. On the contrary, La Niña events would be more favorable to straight-line TC tracks resulting in more SCS TCs (despite generating less TCs in the Pacific basin).

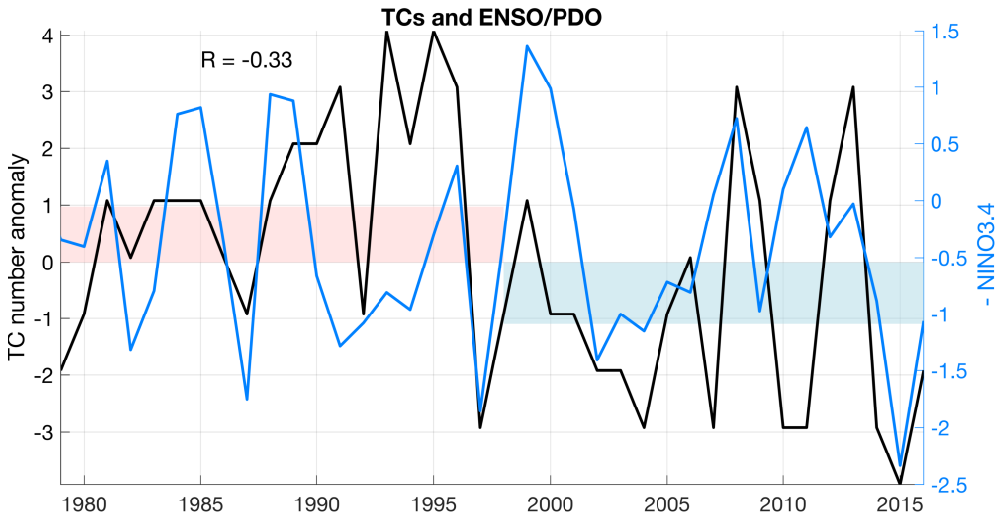

Figure 7: Annual TC numbers anomaly in the SCS during 1979-2016, compared with the negative of Nino3.4 index anomaly. The correlation between TC count and Nino3.4 is -0.33 with 95% confidence. Mean numbers for the warm (1979-1998) and cold (1999-2016) PDO phases are shown in light red and blue shades respectively. There is a difference of 2.1 TCs between phases, much larger than the standard error on the mean of 0.35 TC/yr.

The out-of-phase relationship with the Pacific basin-scale interannual forcing is confirmed

in Figure 8, showing composites of TC density anomalies during the various phases and flavors of ENSO. SCS TC activity varies oppositely with that in the NWP. During EP Niño (La Niña), SCS TC density decreases (increases) in the northern SCS, contrarily to the open-ocean region (the NWP cyclogenesis region is between 120-180E and extends beyond the region shown in Fig. 8). However, the SCS TC density increases in the southern SCS during CP Niños (in phase with the open ocean). This result is substantiated by a regression of SST onto SCS TC density for each cluster (Fig. 9). It unambiguously confirms that TC activity in northern and southern SCS is modulated by different ENSO phases. However, the ENSO-TC correlation remains low in the SCS. The overall Nino3.4-TC correlation is significant but not high at -33%, while TC frequency is correlated at 60% to CP Niños in the NWP, outside the SCS.

The out-of-phase relationship associated with the ENSO-typhoon hypothesis can blur the correlation between ENSO and SCS TC activity, but that can be accentuated by other causes. For example, part of the interannual variability may be stochastic and associated with mesoscale interactions during cyclogenesis (Jourdain et al., 2011; Menkes et al., 2012; Simpson et al., 1997) – as opposed to cyclogenesis environmental factors. Another cause of a weak ENSO control is another out-of-phase relationship between SCS TCs generated locally (a third of all SCS TCs) and remotely in the NWP (Ling et al., 2015). According to Ling et al. (2015), an eastward shift of the western Pacific subtropical high would reduce the number of TCs entering the SCS but favor in the same time local environmental factors of cyclogenesis (essentially a weaker wind shear). A regression of wind shear onto TC number in the NWP, outside the SCS (not shown), seems to confirm this possibility. Therefore, the TC track deviations described in the ENSO-typhoon hypothesis may be opposed by local environmental factors, reducing linear correlations even further.

3.2.2. Decadal modulation

Interestingly, a stronger and opposite relationship prevails between SCS TC frequency and decadal environmental forcing, compared with interannual forcing. A regime shift co-incidental with the PDO phase transition of 1998 is clearly reflected in the SCS TC count

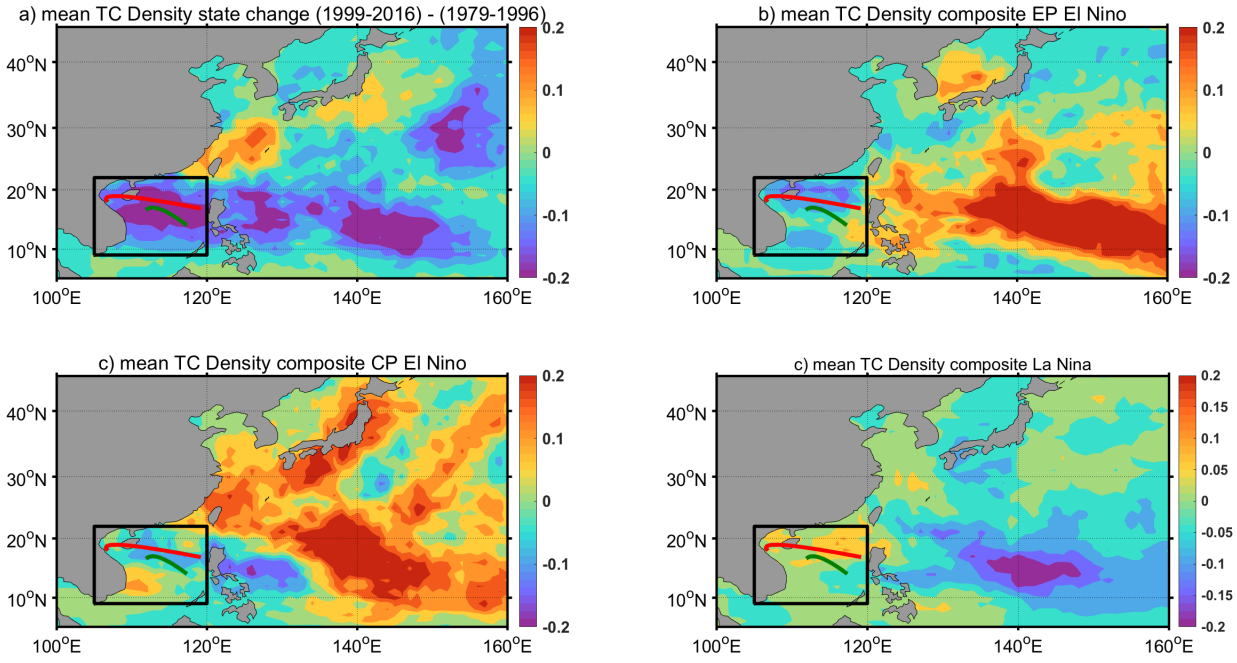

Figure 8: Composite of TC density anomalies (TC number anomalies per 5°x5°). a) Differences between warm and cold PDO phases; b) EP Niño; c) CP Niño; d) La Niña. ENSO Events are chosen according to the Climate Prediction Center classification. Composites are for the summer-fall TC season (May-December); EP El Nino years: 1982, 1986, 1987, 1991, 1997, 2015; CP El Nino years: 1990, 1995, 2002, 2004, 2009; La Nina years: 1983, 1984, 1988, 1989, 1995, 1996, 1998, 1999, 2001, 2007, 2008, 2010, 2011, 2012. Mean tracks for northern and southern clusters are shown in red and green respectively.

(Fig. 7) – as also recently observed in Zhao and Wang (2019) but for the whole NWP basin. The warm PDO phase of 1976-1997 met with an averaged 9.9 TCs per year in the SCS, but only 7.8 TCs per year during the cold phase of 1999-2016, representing a significant 2.1 TCs/yr or $\sim$ 23% difference between the two phases (the standard error of the mean is 0.35 TC/yr). Paradoxically, the cool phase is characterized by both more La Niña and CP Niño events and fewer EP Niños, which is favorable to SCS TCs at interannual time scales (for both Cluster North and South). Therefore, PDO has an overwhelming influence over ENSO on SCS TC frequency. It cannot simply be expressed as an addition of ENSO events of the same phase (Warm PDO/El Nino; cold PDO/La Nina) since, on the contrary, it has an opposite effect to these events. The main reason may lie in the PDO singularity

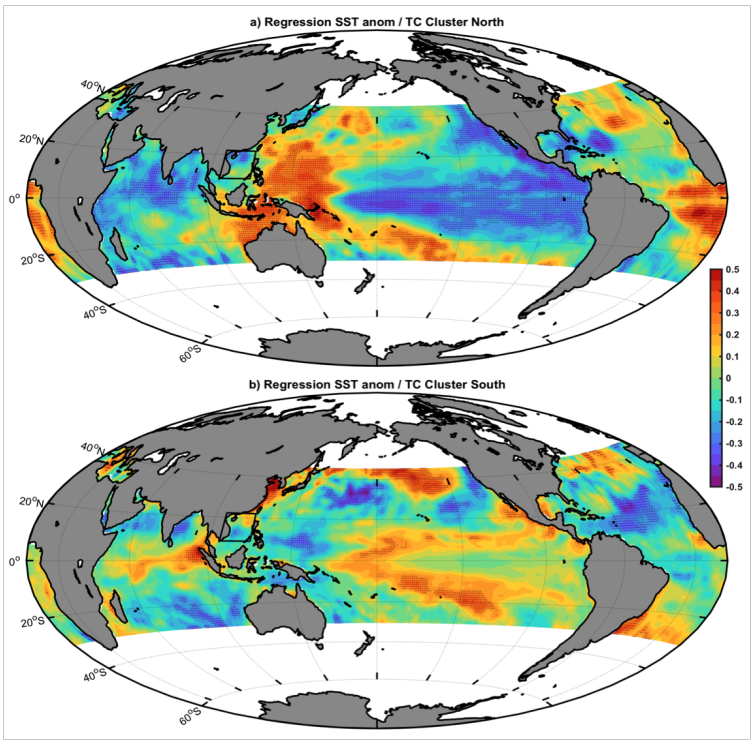

Figure 9: Regression of Pacific SST onto SCS TC number time series for: a) Cluster North, showing a pattern characteristic of La Niña; b) Cluster South, showing a pattern characteristic of CP Niño. Dots indicate significance at the 95% confidence level (Student t-test)

regarding its vertical wind shear pattern in the Central Pacific (Fig. 10). The difference between warm and cool PDO phases shows very unfavorable wind shear in the recent cold phase at longitudes 150-180E (latitudes 10-20N), where a large part of NWP cyclogenesis occurs (see also Zhao and Wang 2019).

In conclusion, our results show that the SCS is in line with the whole NWP cyclogenesis basin at decadal timescales (as *a priori* expected as two thirds of SCS TCs originate from this basin), with significant decrease of TC frequency during the last cool PDO phase. However, at interannual timescales, out-of-phase relationships between local and remote conditions make predictions of cyclogenesis over the SCS particularly challenging. In addition, TC activity in the northern and southern SCS (summer and winter respectively) is modulated by different ENSO phases, which makes it even more confusing. The relations are summarized in Table 1.

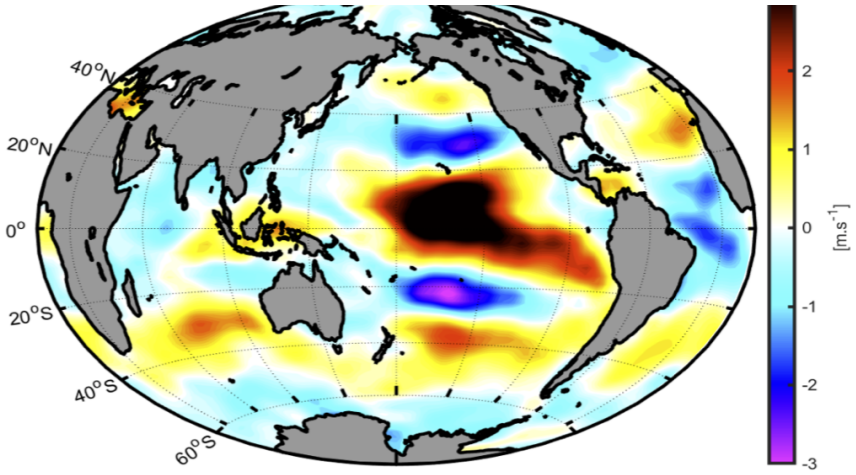

Figure 10: Difference of vertical wind shear between cold (1999-2016) and warm (1979-1996) PDO phases. The dateline is in the center of the map.

3.2.3. Sediment transport contribution

The impact of TCs in terms of longshore sediment transport can be computed by extracting wave conditions during TC activity. To that end, we compose our proxy of coastal vulnerability during days when TC from each cluster are present in the SCS (Fig. 11). Interestingly, the largest contribution to the longshore sediment transport is given by Cluster South, contrarily to the monsoon effect, and is located along the northern and central coast (the effect in the southern region is weak and similar for the two clusters). This result can be associated with the northern side of TCs, which is the most favorable to generate swell traveling toward the coast of Vietnam and southern China (the southern side possibly affecting Malaysia and the Philippines). We thus expect a larger impact of Cluster North along the Chinese coast, further north.

A quantitative comparison between Typhoon and monsoonal effects around Hoi An (Fig. 12) shows that TCs contribute about 15% of the net annual sediment transport to the south. The main contribution is by Cluster South during the start of winter monsoon (from October to December), which adds up to the large winter monsoon southward transport. Cluster North only contributes a small fraction of transport in summer. Because Cluster South is the dominant driver, the variability of TC-induced sediment transport is correlated with

TC Count	EP Niño	CP Niño	La Niña	Warm PDO	Cold PDO
SCS	−	−	+	++	−−
N. SCS	−	−	+	++	−−
S. SCS	No	+	No	++	−−
NWP	+	+	−	++	−−

Table 1: Summary of qualitative TC relationship to ENSO and PDO signals for the whole South China Sea (SCS), the northern and southern subregions (N. SCS and S. SCS) and for the Northwest Pacific basin (NWP). + (−) signs mean positive (negative) correlations, and ++ (−−) means strong correlations.

CP Niños, while the transport driven by winter monsoon is better correlated with La Niña events (Table 1). Therefore, CP Niños tend to modulate the effects of TCs and monsoons on sediment transport in opposite directions. Similarly at decadal scale, the effect of TCs and monsoons on sediment transport are also out-of-phase, as the cold PDO phase is detrimental to TC numbers in the SCS (for both clusters) but favorable to strong winter monsoon waves.

4. Conclusion

Northeast wind monsoon winds are stronger than summer monsoon winds. Accordingly, the highest waves reaching central Vietnam are from the northeast, which suggests that southward longshore transport occurring during winter plays a dominant role in the total sediment budget of central Vietnam. Our estimations show that the annual mean wave energy drives a total longshore sediment transport (longshore drift) in central Vietnam of about 0.5-1 Mm^3/year to the south. We also provide a description and quantification of multi-decadal longshore drift. It shows that strengthening or weakening of the monsoon winds associated with ENSO and PDO phases may have a direct impact on these transports and thus on the erosion process in the region.

The role of ENSO and longer time scales, such as PDO regime shifts, on coastal sediment transport in the SCS has never been identified to our knowledge. The recent decades since 1998 corresponds to a cool PDO phase resembling La Niña pattern, which induces an increase

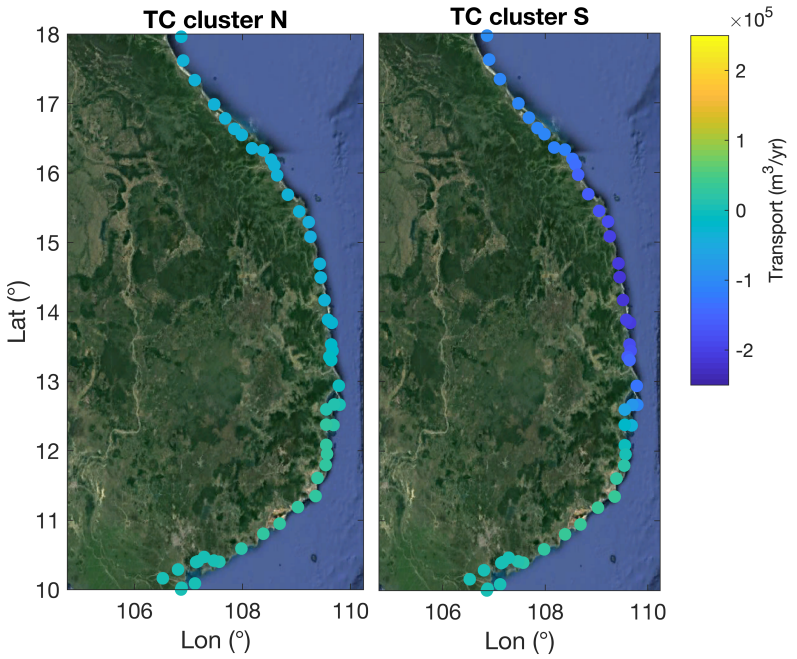

Figure 11: Map of longshore sediment transport due to TCs along the Vietnam coast calculated from ERA-I wave fields and Kaczmarek formulation. Southward transport is negative.

in sediment transport of about 10% associated with increased wave energy in the SCS. The years 1999 and 2011, which experienced particularly strong La Niña events, stand out (40% increase) but other years are also above average from the previous two decades. Coastal erosion results from the divergence of longshore transport (Exner equation), which can vary at the scale of bays according to local geology or man-made coastal developments. Therefore, a natural increase of transport is expected to reflect on coastal erosion and may have played a significant contribution in erosion alerts of this decade such as that of Hoi-An beaches (Nagasawa et al., 2018).

The role of typhoons (and more generally tropical cyclones) in the SCS is also of interest, but their relation to climate modes is more complex. We confirm here for the SCS a reduction of TCs during the last cold PDO phase by 20%. However, contrarily to monsoon modulation, the same phases of ENSO and PDO (cold or warm) have opposite effects on typhoon frequency in the SCS – while they have similar effects in the whole NWP region. The reason appears essentially linked to competing processes affecting TC tracks and cy-

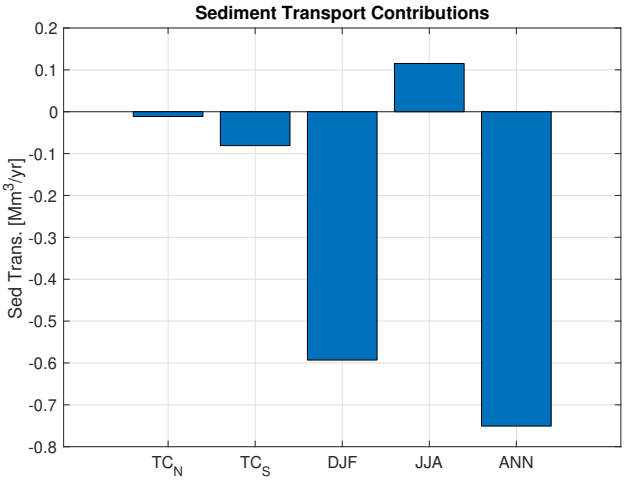

Figure 12: Longshore sediment transport due to TCs along the central Vietnam coast (around Hoi An), comparing annual, seasonal (December-February/DJF and June-August/JJA months for winter and summer respectively) and TC contributions (TC_N and TC_S are for Cluster North and South respectively). Note that the annual transport (ANN) is larger than the net result of DJF and JJA contributions because part of the transport occurs during other months but at lower rates.

clogenesis, as well as local and remote environmental factors. In addition, TC activity in the northern and southern SCS (in summer and winter respectively) are modulated by different ENSO phases (La Niña events favor northern TCs in summer, while CP Niños favor southern TCs in early winter), which makes it even more convoluted.

Nevertheless, it appears that in the last cold PDO phase, a large increase of vertical wind shear in the Central Pacific may have been responsible for the observed decrease in TC activity (20% in the SCS). This decrease is not as clear for stronger typhoons but statistics are less reliable in this case. Interestingly, the PDO cold phase marked both an increase in winter monsoon wave energy and a decrease in TC frequency in the SCS. Therefore, negative impacts that may occur from the former could be compensated by positive impacts of the latter. However, there is no compensation at ENSO time scales, as La Niña events can increase both wave energy (through a reinforcement of winter monsoon) and typhoon occurrence in the SCS.

Interestingly, TCs contribute about 15% of the net annual sediment transport to the south. The main contribution is by southern TC tracks during early winter monsoon (from

October to December), which adds up to the already large winter monsoon southward transport. If TCs and monsoons work together on average, we expect that their sediment transport variability are opposite, both at interannual scale (at least during CP Niños) and at decadal scale, as a cold PDO phase is favorable to strong winter monsoon waves but detrimental to SCS TC numbers.

This study only accounts for climate-modulated wave effects on erosion, dismissing other potentially important processes such as coastal sea level variations, and precipitation affecting both coastal flood events and erosion (e.g., Clift et al. 2015, for paleoclimate effects in the SCS). At seasonal, interannual and decadal scales, wave and wind-driven effects are major drivers of coastal morphology and sea level. Our result may provide predicting information at these scales. For example, if it is confirmed that the strong El Niño of 2015-2016 marked a new regime shift from a cold to a warm PDO phase, we should expect weaker winter monsoons but more frequent TCs. Because monsoon events appear to dominate the coastal response, we may expect a reduction in the general erosion along the Vietnam coast, but possibly an increase in damages caused by winds, waves and precipitation caused by typhoons.

Acknowledgement

This research has received support from the AFD (French Development Agency) in Vietnam. Julien Boucharel is funded by project MOPGA 'Trocodyn' (ANR-17-MPGA-0018) and wants to acknowledge the French Region Occitanie.

References

Almar, R., Kestenare, E., Boucharel, J., 2019. On the key influence of remote climate variability from tropical cyclones, north and south atlantic mid-latitude storms on the senegalese coast (west africa). Environmental Research Communications 1, 071001.

Almar, R., Kestenare, E., Reyns, J., Jouanno, J., Anthony, E., Laibi, R., Hemer, M., Du Penhoat, Y., R., R., 2015. Response of the bight of benin (gulf of guinea, west africa) coastline to anthropogenic and natural forcing, part1: Wave climate variability and impacts on the longshore sediment transport. Continental Shelf Research 110, 48 – 59.

377 Almar, R., Marchesiello, P., Almeida, L., Thuan, D., Tanaka, H., Viet, N., 2017. Shoreline response to a
378 sequence of typhoon and monsoon events. Water 9, 364.
379 Anh, L.T., Takagi, H., Nguyen, D.T., Esteban, M., 2017. Investigation of awareness of typhoon and storm
380 surge in the mekong delta - recollection of 1997 typhoon linda. Journal of Japan Society of Civil Engineers,
381 Ser. B3 (Ocean Engineering) 73, 168–173.
382 Balmaseda, M.A., Mogensen, K., Weaver, A.T., 2013. Evaluation of the ecmwf ocean reanalysis system
383 oras4. Quarterly Journal of the Royal Meteorological Society 139, 1132–1161.
384 Battjes, J.A., Janssen, J.P.F.M., 1978. Energy Loss and Set-Up Due to Breaking of Random Waves. pp.
385 569–587.
386 Bell, S.S., Chand, S.S., Camargo, S.J., Tory, K.J., Turville, C., Ye, H., 2019. Western north pacific tropical
387 cyclone tracks in cmip5 models: Statistical assessment using a model-independent detection and tracking
388 scheme. Journal of Climate 32, 7191–7208.
389 Bird, E., 2005. Drift and Swash Alignments. Springer Netherlands, Dordrecht. pp. 395–397.
390 Boucharel, J., Jin, F.F., England, M.H., Lin, I.I., 2016. Modes of hurricane activity variability in the eastern
391 pacific: Implications for the 2016 season. Geophysical Research Letters 43, 11,358–11,366.
392 Bryan, K., Kench, P., Hart, D., 2008. Multi-decadal coastal change in new zealand: Evidence, mechanisms
393 and implications. New Zealand Geographer 64, 117 – 128.
394 Camargo, S.J., Sobel, A.H., Barnston, A.G., Klotzbach, P.J., 2010. The influence of natural climate vari-
395 ability on tropical cyclones, and seasonal forecasts of tropical cyclone activity, in: Global Perspectives on
396 Tropical Cyclones, pp. 325–360.
397 Capotondi, A., Wittenberg, A.T., Newman, M., Di Lorenzo, E., Yu, J.Y., Braconnot, P., Cole, J., Dewitte,
398 B., Giese, B., Guilyardi, E., Jin, F.F., Karnauskas, K., Kirtman, B., Lee, T., Schneider, N., Xue, Y., Yeh,
399 S.W., 2015. Understanding enso diversity. Bulletin of the American Meteorological Society 96, 921–938.
400 Chang, C.P., Wang, Z., Hendon, H., 2006. The Asian winter monsoon. Springer Berlin Heidelberg, Berlin,
401 Heidelberg. pp. 89–127.
402 Chu, P.C., Qi, Y., Chen, Y., Shi, P., Mao, Q., 2004. South china sea wind-wave characteristics. part i:
403 Validation of wavewatch-iii using topex/poseidon data. Journal of Atmospheric and Oceanic Technology
404 21, 1718–1733.
405 Clift, P.D., Brune, S., Quinteros, J., 2015. Climate changes control offshore crustal structure at south china
406 sea continental margin. Earth and Planetary Science Letters 420, 66 – 72.
407 Dee, D.P., Uppala, S.M., Simmons, A.J., Berrisford, P., Poli, P., Kobayashi, S., Andrae, U., Balmaseda,
408 M.A., Balsamo, G., Bauer, P., Bechtold, P., Beljaars, A.C.M., van de Berg, L., Bidlot, J., Bormann, N.,
409 Delsol, C., Dragani, R., Fuentes, M., Geer, A.J., Haimberger, L., Healy, S.B., Hersbach, H., Holm, E.V.,
410 Isaksen, L., Kallberg, P., Kohler, M., Matricardi, M., McNally, A.P., Monge-Sanz, B.M., Morcrette, J.J.,

Park, B.K., Peubey, C., de Rosnay, P., Tavolato, C., Thepaut, J.N., Vitart, F., 2011. The era-interim reanalysis: configuration and performance of the data assimilation system. Quarterly Journal of the Royal Meteorological Society 137, 553–597.

DeMaria, M., 1996. The effect of vertical shear on tropical cyclone intensity change. Journal of the Atmospheric Sciences 53, 2076–2088.

Elsner, J.B., Liu, K.b., 2003. Examining the enso-typhoon hypothesis. Climate Research 25, 43–54.

Felix, Hernández-Fontes, Lithgow, Mendoza, Posada, Ring, Silva, 2019. Wave energy in tropical regions: Deployment challenges, environmental and social perspectives. Journal of Marine Science and Engineering 7, 219.

Gaffney, S.J., Robertson, A.W., Smyth, P., Camargo, S.J., Ghil, M., 2007. Probabilistic clustering of extratropical cyclones using regression mixture models. Climate Dynamics 29, 423–440.

Hue, N.H., Thanh, N.H., 2020. Assessing the impact of massive development of beach resorts on current status of coastal erosion along the central coast of vietnam, in: Trung Viet, N., Xiping, D., Thanh Tung, T. (Eds.), APAC 2019, Springer Singapore, Singapore. pp. 551–556.

Jourdain, N.C., Marchesiello, P., Menkes, C.E., Lefèvre, J., Vincent, E.M., Lengaigne, M., Chauvin, F., 2011. Mesoscale simulation of tropical cyclones in the south pacific: Climatology and interannual variability. Journal of Climate 24, 3–25.

Kaczmarek, L.M., Ostrowski, R., Pruszak, Z., Rozynski, G., 2005. Selected problems of sediment transport and morphodynamics of a multi-bar nearshore zone. Estuarine, Coastal and Shelf Science 62, 415 – 425. The European contribution to global coastal zone research: An ELOISE (European Land-Ocean Interaction Studies) project.

Kaplan, J., DeMaria, M., 2003. Large-scale characteristics of rapidly intensifying tropical cyclones in the north atlantic basin. Weather and Forecasting 18, 1093–1108.

Komar, P., 1976. Beach Processes and Sedimentation. Prentice-Hall. URL: https://books.google.fr/books?id=-vNOAAAAMAAJ.

Lin, I., Camargo, S., Patricola, C., Boucharel, J., Chand, S., Klotzbach, P., Chan, J., Wang, B., Li, T., F.F., J., 2020. ENSO and Tropical Cyclones. chapter 17, in press.

Ling, Z., Wang, G., Wang, C., 2015. Out-of-phase relationship between tropical cyclones generated locally in the south china sea and non-locally from the northwest pacific ocean. Climate Dynamics 45, 1129–1136.

Lionello, P., Gunther, H., Janssen, P.A.E.M., 1992. Assimilation of altimeter data in a global third-generation wave model. Journal of Geophysical Research: Oceans 97, 14453–14474.

Luijendijk, A., Hagenaars, G., Ranasinghe, R., Baart, F., Donchyts, G., Aarninkhof, S., 2018. The state of the world's beaches. Scientific Reports 8, 6641.

Mantua, N.J., Hare, S.R., 2002. The pacific decadal oscillation. Journal of Oceanography 58, 35–44.

445 Mantua, N.J., Hare, S.R., Zhang, Y., Wallace, J.M., Francis, R.C., 1997. A pacific interdecadal climate
446 oscillation with impacts on salmon production*. Bulletin of the American Meteorological Society 78,
447 1069–1080.
448 Marchesiello, P., Nguyen, N.M., Gratiot, N., Loisel, H., Anthony, E.J., Dinh, C.S., Nguyen, T., Almar,
449 R., Kestenare, E., 2019. Erosion of the coastal mekong delta: Assessing natural against man induced
450 processes. Continental Shelf Research 181, 72 – 89.
451 Menkes, C.E., Lengaigne, M., Marchesiello, P., Jourdain, N.C., Vincent, E.M., Lefèvre, J., Chauvin, F.,
452 Royer, J.F., 2012. Comparison of tropical cyclogenesis indices on seasonal to interannual timescales.
453 Climate Dynamics 38, 301–321.
454 Minderhoud, P.S.J., Coumou, L., Erkens, G., Middelkoop, H., Stouthamer, E., 2019. Mekong delta much
455 lower than previously assumed in sea-level rise impact assessments. Nature Communications 10, 3847.
456 Mirzaei, A., Tangang, F., Juneng, L., Mustapha, M.A., Husain, M.L., Akhir, M.F., 2013. Wave climate
457 simulation for southern region of the south china sea. Ocean Dynamics 63, 961–977.
458 Mortlock, T.R., Goodwin, I.D., 2016. Impacts of enhanced central pacific enso on wave climate and headland-
459 bay beach morphology. Continental Shelf Research 120, 14 – 25.
460 Nagasawa, T., Thuy, M.T.T., Nguyen, T.V., Tanaka, H., 2018. Analysis of shoreline change in cua dai beach
461 by using empirical orthogonal function. Coastal Engineering Journal 60, 548–565.
462 Ngo, N., Tien, C., Pham, H., Do, D., N.B., N., 2006. Status of coastal erosion in Vietnam and measures for
463 protection. Technical Report. Food and Agriculture Organization.
464 Nguyen, N.M., Marchesiello, P., Lyard, F., Ouillon, S., Cambon, G., Allain, D., Dinh, V.U., 2014. Tidal
465 characteristics of the gulf of tonkin. Continental Shelf Research 91, 37–56.
466 Pilkey, O., Cooper, A., 2002. Longshore transport volumes: A critical view. Journal of Coastal Research
467 36, 572–580.
468 Shoji, T., Kanno, Y., Iwasaki, T., Takaya, K., 2014. An Isentropic Analysis of the Temporal Evolution of
469 East Asian Cold Air Outbreaks. Journal of Climate 27, 9337–9348.
470 Simpson, J., Ritchie, E., Holland, G.J., Halverson, J., Stewart, S., 1997. Mesoscale Interactions in Tropical
471 Cyclone Genesis. Monthly Weather Review 125, 2643.
472 Sterl, A., Caires, S., 2005. Climatology, variability and extrema of ocean waves: The web-based knmi/era-40
473 wave atlas. International Journal of Climatology 25, 963–977.
474 Stopa, J.E., Cheung, K.F., 2014. Intercomparison of wind and wave data from the ecmwf reanalysis interim
475 and the ncep climate forecast system reanalysis. Ocean Modelling 75, 65 – 83.
476 Trenberth, K.E., Stepaniak, D.P., 2001. Indices of el niño evolution. Journal of Climate 14, 1697–1701.
477 Wang, G., Su, J., Ding, Y., Chen, D., 2007. Tropical cyclone genesis over the south china sea. Journal of
478 Marine Systems 68, 318 – 326.

Wu, L., Su, H., Fovell, R.G., Wang, B., Shen, J.T., Kahn, B.H., Hristova-Veleva, S.M., Lambrigtsen, B.H., Fetzer, E.J., Jiang, J.H., 2012. Relationship of environmental relative humidity with north atlantic tropical cyclone intensity and intensification rate. Geophysical Research Letters 39.

Zhao, H., Wang, C., 2019. On the relationship between enso and tropical cyclones in the western north pacific during the boreal summer. Climate Dynamics 52, 275–288.